Field Quality of the Series of Short Orbit Nested Corrector Magnets for HL-LHC

M. Domínguez, O. Durán, J. García, J. A. García-Matos, L. García-Tabarés, Luis González, R. López, T. Martínez, C. Martins Jardim, J. M. Pérez, F. Toral, J. Ferradas, L. Fiscarelli, G. Hernando, J. C. Pérez, S. Izquierdo, E. Todesco, and G. Willering

***Abstract*—MCBXF magnets are orbit correctors for the High-Luminosity (HL) Large Hadron Collider (LHC) upgrade. The magnet design consists of two nested dipoles, with an aperture of 150 mm, which is described elsewhere. The magnets have been designed in two physical lengths, namely of 2.5 m (MCBXFA) and 1.5 m (MCBXFB), with the same cross section. The series production of the magnets consists of 5 long and 10 short magnets. The component production is being carried out at CIEMAT and magnet assembly is made at CERN. This paper summarizes the results of the magnetic measurements of the short magnets produced so far, including warm magnetic measurements. The first magnets featured repetitive results regarding field quality. Afterwards, some of the magnets showed a shift of the main harmonics. After careful analysis of the fabrication steps, it was found out that the impregnation mold assembly strategy impacted on the coil dimensions. The shimming plan was tuned to deal with this feature, and the field quality was enhanced accordingly.**

***Index Terms*—HL-LHC, MCBXF, nested superconducting dipole, superconducting magnet tests, magnetic measurements, shimming plan.**

I. Introduction

THE High-Luminosity LHC (HL-LHC) project aims to push the LHC scientific scope beyond its current limits. Such an upgrade will imply the implementation of the MCBXF orbit correctors, arranged in a nested dipole configuration. They are equipped with a custom collar structure in order to lock the torque due to the large Lorentz forces that appear during combined operation. Each NbTi dipole acts on the horizontal and vertical plane respectively. The 2.5 m long (MCBXFA) and 1.5 m long (MCBXFB) versions are to be produced [1], sharing the same cross section, depicted in Fig. 1. More precisely a total of 5 long and 10 short series magnets are to be delivered. So far, a total of 8 magnets of the MCBXFB series and 3 of the MCBXFA have been produced. Magnetic, mechanical and engineering design of these magnets, as well as their main parameters and magnet protection strategy are detailed in [2], [3], [4], [5], [6].

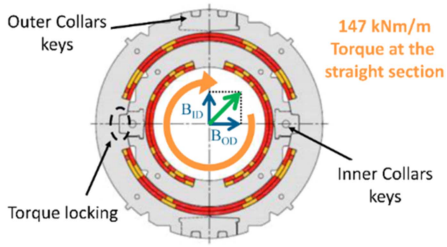

Fig. 1. Cross section of MCBXFB collared coils. Torque locking with nested collaring for combined operation is highlighted.

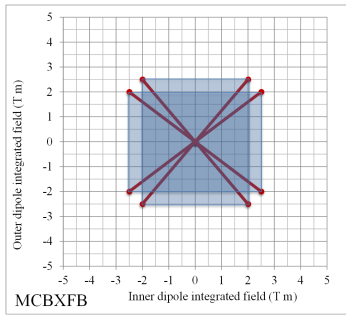

Fig. 2. Operational nominal space for MCBXFB magnets.

This paper shows the results of the magnetic measurement campaigns performed at room temperature (RT) and 1.9 K on the magnets MCBXFB01 to B08. The reference radius is 50 mm. Fig. 2 shows the nominal operational range. The diagonals are the powering ramps followed for the magnetic measurements. Ultimate integrated field is 2.678 T·m [7].

In terms of field quality, the beam optics requires as acceptance limits that all integral multipoles of the magnets at

Received 28 July 2025; revised 11 September 2025; accepted 12 September 2025. Date of publication 23 October 2025; date of current version 4 November 2025. This work was supported in part by the Spanish Center for Technological and Industrial Development (CDTI), in part by the Spanish Ministry of Science and Innovation through PRISMAC Program (2019, March 26th), and in part CERN under Contract KE-3797. *(Corresponding author: Luis González.)*

M. Domínguez, O. Durán, J. García, L. García-Tabarés, Luis González, R. López, T. Martínez, C. Martins Jardim, J. M. Pérez, and F. Toral are with the Centro de Investigaciones Energéticas, Medioambientales y Tecnológicas (CIEMAT), 28040 Madrid, Spain (e-mail: manuel.dominguez@ciemat.es; oscar.duran@ciemat.es; javier.garcia@ciemat.es; luis.garcia@ciemat.es; luis.gonzalez@ciemat.es; ricardo.lopez@ciemat.es; teresa.martinez@ciemat.es; carla.martins@ciemat.es; jm.perez@ciemat.es; fernando.toral@ciemat.es).

J. A. García-Matos is with CIEMAT, 28040 Madrid, Spain, and also with the ICAI School of Engineering, Comillas Pontifical University, 28015 Madrid, Spain (e-mail: jesusangel.garcia@ciemat.es).

J. Ferradas, L. Fiscarelli, G. Hernando, J. C. Pérez, S. Izquierdo, E. Todesco, and G. Willering are with CERN, 1211 Geneva, Switzerland (e-mail: jose.ferradas.troitino@cern.ch; lucio.fiscarelli@cern.ch; gonzalo.hernando.irisarri@cern.ch; juan.carlos.perez@cern.ch; susana.izquierdo.bermudez@cern.ch; ezio.todesco@cern.ch; gerard.willering@cern.ch).

Color versions of one or more figures in this article are available at https://doi.org/10.1109/TASC.2025.3624733.

Digital Object Identifier 10.1109/TASC.2025.3624733

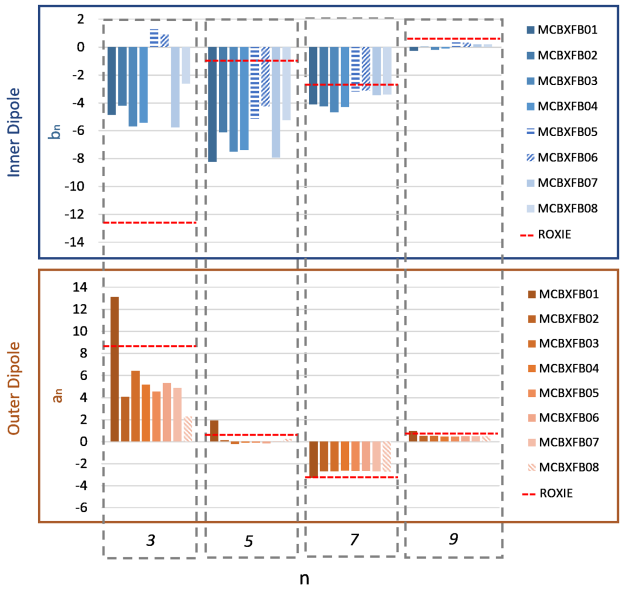

Fig. 3. Integrated main allowed multipoles measured for MCBXFB01 to B08. Upper panel: Inner Dipole. Lower panel: Outer dipole. Red dashed line represents the nominal values calculated with Roxie.

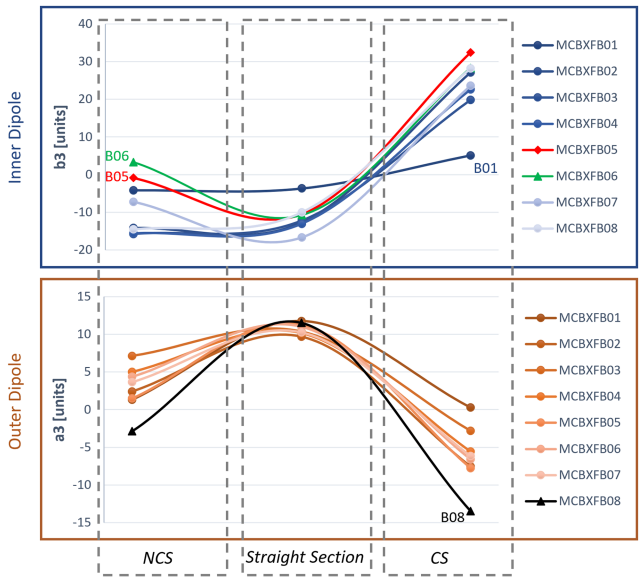

Fig. 4. Main allowed multipoles measured at three different positions along the axis of MCBXFB02-08 magnets. Upper panel: Inner Dipole. Lower panel: Outer dipole.

1.9 K shall be smaller than 5 units (0.05%) normalized with respect to the nominal integrated field [9]. The acceptance limit for the sextupoles a_3 and b_3 is 20 units, while it is 7 units for the decapoles a_5 and b_5 . This exceptions are intended to comply with the effect of the iron saturation in the wide range of powering scenarios.

II. Magnetic Measurements

Magnetic measurements were performed both at RT during the assembly process and 1.9 K after the complete magnet assembly. The reference system was chosen so that the main field direction (B1) is aligned with the dipole field generated by the inner dipole (ID).

A. Warm Magnetic Measurements

RT measurements were carried out after each dipole collaring for quality control, and finally after iron assembly. They are made by using a dedicated testbench equipped with a horizontal rotating coil at a reference radius of 50 mm. The accuracy of the magnetic measurements is about 1 ppm [8]. The coils are powered at a constant current of 5 A. Upper and lower panels of Fig. 3 show, for magnets MCBXFB01 to 08, a summary of the main integrated multipoles for individual powering of the inner and outer dipole, respectively, after final magnet assembly. The results are compared with the nominal values calculated with Roxie [9]. The magnets were assembled and tested sequentially, in ascending order. Here we present a chronological analysis of the results.

The values of the integrated b_3 of the inner dipole of magnets B01 to B04 were consistently showing an average value of around -5 units with a low relative variability. At that moment, it was decided to keep these small values of b_3 at low currents, which is the most likely range of operation for a corrector magnet. Nominal multipole values were aimed to center the variation of the multipoles with current in the whole operational space. Since there is only one design variable, the shimming distribution between midplane and pole turn, the value of b_5 increased accordingly when optimizing b_3 . The sextupoles are very sensitive to a tangential displacement of the coils: 0.1 mm of tangential shift yields 7 units for the inner dipole and 2.2 units for the outer one.

After measurement of B05 magnet, the results showed a b_3 shift of around 6 units. Such discrepancy was observed again for B06.

Regarding outer dipoles, the measured a_3 of B01 was larger, but within the acceptance limits. The next magnets performed small multipoles. There is a shift of around 2 units for magnet B08, which could have a similar origin to the shift observed for the inner dipoles of B05 and B06 magnets.

In order to understand the origin of the observed anomalies in the integrated b_3 and a_3 values, the field quality at different points along the magnets was analyzed. The resolution of the scan is limited to the length of the rotating coil, i.e., 600 mm, allowing for 3 measurements, one at the straight section and one at each extremity of the magnet, corresponding to the coil ends at the Connection Side (CS) and Non-Connection Side (NCS). Upper and lower panels of Fig. 4 show the measurements.

In the case of the inner dipole, it can be noticed that for B05 and B06, the value of b_3 diverge from the previous tendency mainly at the NCS. This information was very important for the corrective actions implemented for B07 and B08, as it will be explained in the next Section.

Regarding the outer dipole, a deviation of around 5 units in a_3 for B08 can be seen at both NCS and CS.

TABLE I
MAXIMUM CURRENTS AT EACH POWERING CYCLE

	Scan_ID		Scan_OD		ID + 80%OD		OD + 80%ID	
	%	I [A]	%	I [A]	%	I [A]	%	I [A]
ID	100	1740	0	0	100	1740	80	1400
OD	0	0	100	1430	80	1135	100	1430

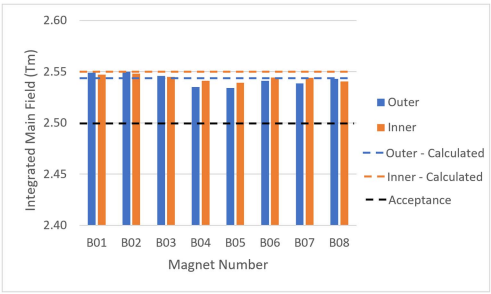

Fig. 5. Integrated field for inner and outer dipoles of B01 to B08 magnets. Dashed lines represent calculated and acceptance values.

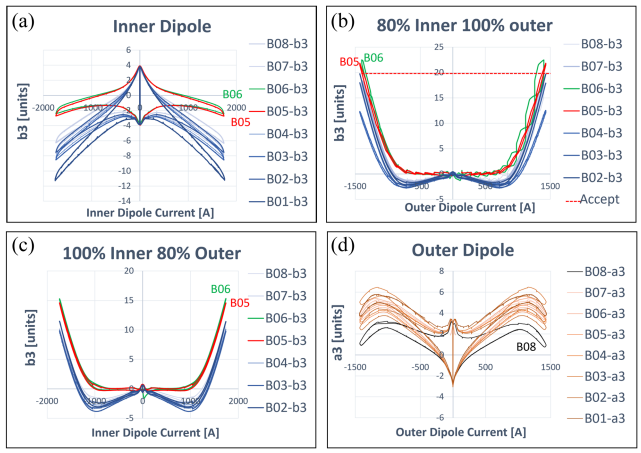

Fig. 6. MCBXFB02-08 integrated multipoles b_3 and a_3 measured at different powering scenarios.

B. Cold Magnetic Measurements

To confirm the fulfillment of the field quality acceptance limits, after magnet assembly, the magnets are inserted in a vertical cryostat in the so-called cluster D of SM18 test facility at CERN. The cold magnetic measurements were performed at different powering scenarios with various combinations of maximum current at the inner (ID) and outer (OD) dipoles, as depicted in Table I. The powering ramps follow the diagonals shown in Fig. 2. A shaft with five segments of 500-mm-long rotating coils at a reference radius of 50 mm was used.

The integrated dipole fields of each magnet are presented in Fig. 5 in comparison with the acceptance limit and the calculated values. The results show high repeatability and very good accordance with calculations. The fields are higher than the acceptance (minimum) value, since the iron saturation is small in standalone operation.

Multipole normalization must be carefully addressed in the case of MCBXF magnets during combined powering. The standard normalization strategy for individual dipoles is based on the use of the value of the main multipole A_1 and B_1 at each powering stage:

$$b_n = 10^4 \times \frac{B_n}{B_1} \qquad a_n = 10^4 \times \frac{A_n}{A_1} \tag{1}$$

However, by following this strategy during combined operation, depending on which magnetic field is assumed to be the main component, normal multipoles b_n would be normalized to the skew main field A_1 and vice versa. A reasonable alternative is based on the use of the constant value of the nominal integrated field, i.e., 2.5 Tm, as the reference field. However, this normalization carries an inconvenience: when normalizing to a constant value, the sign of the multipoles would depend on the sign of the current, and this should not be the case. Therefore, the normalization strategy is finally based on using the constant value of the nominal integrated field multiplied by the signum function of the powering transfer function (TF):

$$b_n = sgn\,(TF) \times 10^4 \times \frac{B_n}{2.5} \quad a_n = sgn\,(TF) \times 10^4 \times \frac{A_n}{2.5} \tag{2}$$

Fig. 6 shows a summary of the most relevant results of magnetic field quality for the different powering scenarios. It is important to notice that the iron saturation during cold powering plays a major role in the field quality. As it was pointed out in the previous Section, the multipoles are small for low currents, increasing noticeably for high currents, mainly due to the outer dipole one. Only few points at the powering scenario "80% Inner + 100% Outer" lay slightly out of the acceptance range, linked to the reported multipole shift of B05 and B06 inner dipole. Nevertheless, these results are still acceptable for the machine operation.

A clear correlation can be found between warm magnetic measurements and single powering cold magnetic measurements at full current, i.e., in absence of wire magnetization effects. The latter confirms that warm data are a very good predictor, and a valuable asset for magnet characterization during assembly.

III. SHIMMING PLAN

As pointed out in the previous Section, the field quality is very sensitive to the coil dimensions, mainly in azimuthal direction. The coils are fully impregnated in epoxy resin, with a smeared-out modulus of elasticity around 20–25 GPa [10]. The target preload at the collaring press is about 160 MPa, with a tolerance of +/- 20 MPa [6]. It implies an accuracy better than 0.1 mm for the collared coil assembly. Therefore, the coil dimensions need to be measured with a precision in the order of a few hundredths of mm. It is made by means of a coordinate measuring machine (CMM). The coil is fixed to a precision tooling to eliminate the natural bending in free state.

From Fig. 4, it can be concluded that the main multipole shift is at the NCS, and also at CS, but less intense in the latter case. This could be explained because the rigidity of the end spacers at the coil heads is different: they are split at CS, which is indeed less rigid. The multipoles b_3 and b_5 at

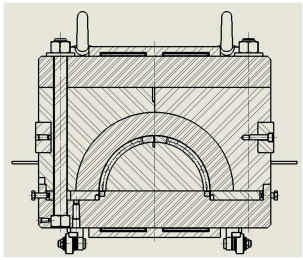

Fig. 7. Cross section of the impregnation mold for inner dipole coils.

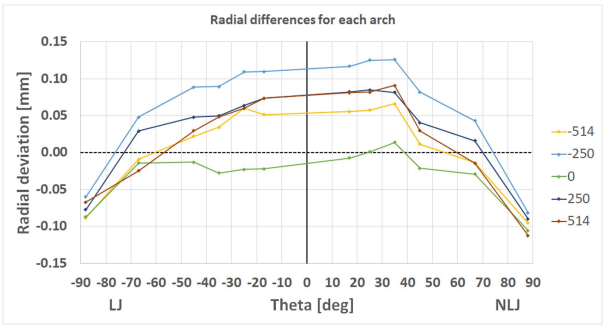

Fig. 8. Deviation from the nominal position of the outer face of the coil in radial direction, at different angular positions for five positions along the coil axis.

the central segment are shifted towards more positive values. This signature is compatible with a displacement of the cable blocks towards the midplane, as confirmed by electromagnetic simulations performed with Roxie.

The final dimensions of the coils are dominated by the impregnation mold. During the production of the coils for magnets B05 and the following ones, it was noticed that some parts of the mold were not in perfect contact, with gaps of a few hundredths of mm (Fig. 7). It was not further investigated by that time, assuming that they were small.

When the deviations on the field quality of magnets B05 and B06 were noticed, a more careful investigation revealed that these gaps could create an excess of volume for the coil ends which would be filled with resin, mainly around the pole window. This feature was not detected by the CMM because the outer face of the coils was not measured, assuming that the impregnation mold was completely close, determining precisely the outer radius of the coil. Fig. 8 shows the radial deviation from the nominal position of the outer face of a coil impregnated with a mold not completely closed. One can notice that the central section of the coil ("0" label) is at nominal position, while there is an increasing excess of resin towards the ends ("514" label, which is the distance from the center in mm).

This excess of coil volume was not considered for the shimming plan of magnets B05 and B06, yielding an excessive pressure of the collars on the coils, which would shift the cable blocks towards the midplane, mainly at the coil heads.

Two corrective actions were implemented for the next coils:

1) The impregnation mold parts were carefully checked and repaired. There were some scratches due to the aging after several uses.

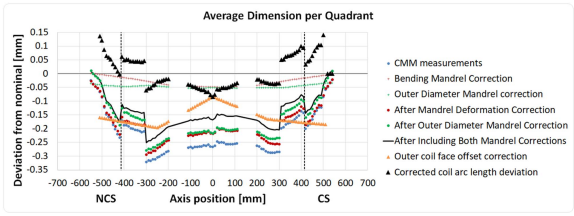

Fig. 9. Corrections on CMM measurements of coil ICBS21, including the mandrel deformation and the excess of resin in radial direction.

2) The outer face of the coils is also measured with the CMM, and these measurements are included in the calculations of the shimming plan of the next magnets.

Fig. 9 shows the importance of including the measurement of the outer face of the coil on the computed dimension of the arc length of inner dipole coil ICBS21 (example of a coil where the mold was not completely closed). Initially, the CMM probe measures the position of the midplane and the pole window of the coil. The coil is clamped onto the winding mandrel to avoid the natural bending in free state and ease the comparison with the nominal geometry. Since the mandrel is not a perfect piece, both its bending and the deviation from the nominal geometry are measured to correct the measurements performed on the coil. Finally, the measurements on the outer surface of the coil are used to find the right value of the arc length of the coil, which is the dimension used to define the shimming thickness to be added both at the midplane and the pole window to achieve the preload target while keeping a good field quality.

From Fig. 4, one can notice that the distribution of b_3 along the magnet axis is not the same for magnet B07 than in the first series magnets, but the integrated value is quite close. In the case of B08, the distribution is similar to the first magnets. Therefore, this strategy will be kept for the rest of the series magnets. Finally, one can notice a similar signature in the multipole distribution along the axis of the outer dipole of magnet B08. In consequence, the same corrective actions will be implemented for the next outer dipole coils.

IV. Conclusion

CIEMAT is contributing to HL-LHC project with the production of the nested orbit corrector magnets, in two lengths. This paper reports about the magnetic field quality of the short ones, namely MCBXFB. Eight out of ten series magnets have been successfully produced and tested. Two of them, B05 and B06, showed some deviation of the b_3 and b_5 multipoles with respect to the previous ones. After careful investigation, it was found that the aging of the impregnation mold impacted on the final dimensions of the coils. Corrective actions have been successfully implemented in the quality control procedure. In case of excessive dimension of the impregnated coils, it could be compensated with the shimming plan.

Acknowledgment

The authors would like to thank both the whole CIEMAT and CERN teams working on component production and magnet assembly, respectively, and the SM18 test facility team (CERN).

REFERENCES

[1] E. Todesco et al., "A first baseline for the magnets in the high luminosity LHC insertion regions," *IEEE Trans. Appl. Supercond.*, vol. 24, no. 3, Jun. 2014, Art. no. 4003305, doi: 10.1109/TASC.2013.2288603.

[2] J. A. Garcia-Matos et al., "Detailed magnetic and mechanical design of the nested orbit correctors for HL-LHC," *IEEE Trans. Appl. Supercond.*, vol. 28, no. 3, Apr. 2018, Art. no. 4101005, doi: 10.1109/TASC.2017.2784806.

[3] J. A. García-Matos et al., "Fabrication and power test of the second MCBXFB nested orbit corrector prototype for HL-LHC," *IEEE Trans. Appl. Supercond.*, vol. 31, no. 5, Aug. 2021, Art. no. 4000605, doi: 10.1109/TASC.2021.3059610.

[4] F. Toral et al., "Protection strategy and quench study of MCBXF magnets," *IEEE Trans. Appl. Supercond.*, vol. 32, no. 6, Sep. 2022, Art. no. 4004005, doi: 10.1109/TASC.2022.3159776.

[5] J. A. García-Matos et al., "Fine tuning of the inner dipole design of MCBXF magnets," *IEEE Trans. Appl. Supercond.*, vol. 32, no. 6, Sep. 2022, Art. no. 4000405, doi: 10.1109/TASC.2022.3148688.

[6] C. M. Jardim et al., "Fabrication and power test of last MCBXFB magnets," *IEEE Trans. Appl. Supercond.*, vol. 32, no. 6, Sep. 2022, Art. no. 4007006, doi: 10.1109/TASC.2022.3175151.

[7] E. Todesco, J. C. Pérez, and F. Toral, "Acceptance criteria of CIEMAT in-kind contribution (MCBXF nested orbit corrector magnets) | document LHC-MCBXFA-ES-0002 (v.1.1)," Mar. 2022. Accessed: Sep. 09, 2022 . [Online]. Available: https://edms.cern.ch/document/2051311/1.1

[8] J. DiMarco et al., "Application of PCB and FDM technologies to magnetic measurement probe system development," *IEEE Trans. Appl. Supercond.*, vol. 23, no. 3, Jun. 2013, Art. no. 9000505, doi: 10.1109/TASC.2012.2236596.

[9] S. Russenschuck, M. Aleksa, C. Völlinger, S. Ramberger, J. Lucas, and M. Bazan, "Integrated design of superconducting magnets with the CERN field computation program ROXIE," 2000. Accessed: Feb. 10, 2014. [Online]. Available: http://cds.cern.ch/record/480810/files/lhc-project-report-446.pdf

[10] J. A. García-Matos, "Nested cos-theta superconducting accelerator dipoles with high radiation resistance: Application to the HL-LHC orbit correctors," Ph.D. thesis, Universidad Politécnica de Madrid, Madrid, Spain, 2022, doi: 10.20868/UPM.thesis.72080.